PNAS RESEARCH ARTICLE | ENGINEERING MICROBIOLOGY

A 3D-printed transepidermal microprojection array for human skin microbiome sampling

Kun Liang[a,1,2], Cheryl Leong[a,2], Jia Min Loh[a], Nathania Chan[a], Larissa Lim[a], Yuen In Lam[a], Thomas L. Dawson Jr.[a,b,c], and Hong Liang Tey[d,e,f]

Edited by Joseph DeSimone, Stanford University, CA; received February 28, 2022; accepted June 6, 2022

Skin microbiome sampling is currently performed with tools such as swabs and tape strips to collect microbes from the skin surface. However, these conventional approaches may be unable to detect microbes deeper in the epidermis or in epidermal invaginations. We describe a sampling tool with a depth component, a transepidermal microprojection array (MPA), which captures microbial biomass from both the epidermal surface and deeper skin layers. We leveraged the rapid customizability of 3D printing to enable systematic optimization of MPA for human skin sampling. Evaluation of sampling efficacy on human scalp revealed the optimized MPA was comparable in sensitivity to swab and superior to tape strip, especially for nonstandard skin surfaces. We observed differences in species diversity, with the MPA detecting clinically relevant fungi more often than other approaches. This work delivers a tool in the complex field of skin microbiome sampling to potentially address gaps in our understanding of its role in health and disease.

skin microbiome sampling | microprojection array | 3D printing

Significance

Conventional skin microbiome samplings performed using swabs and tape strips are limited by their abilities to collect microbes solely from the skin surface, rather than from the deeper epidermal regions. A human skin microbiome sampling tool with a transepidermal sampling component, microprojection array (MPA), was developed through a systematic optimization process enabled by 3D printing. MPA sampling of human scalp showed higher fungal diversity and was more effective in extracting fungi belonging to the *Ascomycota* phylum compared to existing methods, demonstrating its role in supporting future clinical diagnosis of skin microbial infections.

The skin microbiome comprises diverse families of microbes that play a complex role in skin health and disease. Skin microbiome sampling is widely used for characterization and study of the human skin microbiome to understand the composition and role of different microbial communities as commensals, mutualists, or pathogens (1). In the clinic, sampling of skin microbes is needed to determine if the administration of antimicrobial or antifungal therapy is required. Asymptomatic microbial skin colonization has been identified as a risk factor for subsequent bloodstream infection (2). Notably, commensal bacteria such as *Staphylococcus aureus* (*S. aureus*) can cause severe skin and tissue infection, which is a major contributor to hospital-acquired infections and mortality (3). Similarly, commensal fungi such as *Candida* and *Dermatophytes* may also cause chronic superficial and cutaneous fungal infections such as tinea pedis, pityriasis versicolor, and candidiasis (4).

The stratum corneum (SC) is the uppermost layer of the epidermis and forms our first line of microbial defense. It comprises corneocytes in layers 10 to 15 cells thick and 10 to 20 μm deep that are held together by tight epidermal junctions. Contrary to popular belief, microbial colonization at the SC is not uniformly two-dimensional (i.e., only on skin surface) but is instead distributed across various compartments in the deeper layers including hair follicles, sweat, and sebaceous glands (5–7). It is postulated that skin surface microbes are transient and that the bacteria in deeper epidermal and dermal regions should be regarded as the host indigenous microbiome (8). Using serial tape stripping, it has been established by 16S amplicon sequencing that bacteria populate the upper SC layers but become scarcer farther down the SC (9, 10). Species such as *S. aureus* strains associated with atopic dermatitis have been observed to increase in relative abundance in deeper layers of the skin (11). It was also demonstrated that bacterial species composition varies with the thickness of the SC, the presence of hair follicles, and other axillary appendages (12). To our knowledge, there have been no studies describing changes in commensal fungi composition in human skin assessed by depth. The highly resistant pathogen *C. auris* has been detected in the deeper layers of mouse skin up to 4 mo after initial colonization, despite the mice being negative for *C. auris* with a skin swab (13). Attempts to characterize the deeper human skin microbiome by biopsy have shown that several bacteria species such as *Clotridiales* and *Bacteriodetes* are enriched in biopsies (14). These findings suggest that the deeper epidermal regions comprise a distinct microbial niche that warrants further investigation.

Current skin sampling methods such as swabbing and tape stripping are limited by their abilities to collect samples solely from the skin surface or SC of the epidermis (15–17). Such samples may not accurately reflect the entire spectrum of microbes present, potentially leading to false negative diagnosis of pathogenic species. Punch biopsies offer a better representation of skin microbiota in deeper layers, including the

Author affiliations: [a]A*STAR Skin Research Labs (A*SRL), Agency for Science, Technology and Research (A*STAR), Singapore 138648; [b]College of Pharmacy, Department of Drug Discovery, Medical University of South Carolina, Charleston, SC 29425 USA; [c]Skin Research Institute of Singapore (SRIS), Singapore 308232; [d]National Skin Centre (NSC), Singapore 308205; [e]Lee Kong Chian School of Medicine, Nanyang Technological University, Singapore; and [f]Yong Loo Ling School of Medicine, National University of Singapore, Singapore

Author contributions: K.L. and C.L. designed research; K.L., C.L., J.M.L., N.C., and L.L. performed research; K.L., C.L., T.L.D.J., and H.L.T. contributed new reagents/analytic tools; K.L., C.L., J.M.L., N.C., L.L., Y.I.L., and T.L.D.J. analyzed data; and K.L., C.L., T.L.D.J., and H.L.T. wrote the paper.

The authors declare no competing interest.

This article is a PNAS Direct Submission.

[1]To whom correspondence may be addressed. Email: kun_liang@asrl.a-star.edu.sg.

[2]K.L. and C.L. contributed equally to this work.

This article contains supporting information online at http://www.pnas.org/lookup/suppl/doi:10.1073/pnas.2203556119/-/DCSupplemental.

Published July 22, 2022.

dermis, but are invasive and painful (14, 15, 18). Hence, there is a need for innovative, minimally invasive sampling tools to reliably assess the microbiome across the superficial epidermis layers to deeper layers of the dermis.

Microprojection arrays (MPAs), also known as microneedles, are minimally invasive medical devices comprising an array of three-dimensional (3D) microstructures intended to overcome the skin barrier for transdermal delivery or skin diagnostics (19–21). While there has been extensive research on MPAs for biofluid collection (22–24), studies on application of MPAs for cellular and microbial material retrieval from skin have been limited to date. To our knowledge, there have been no prior reports on using MPA to enable adhesion-based transepidermal microbiome sampling. We hypothesize the penetration of MPAs into underlying skin layers renders MPA a suitable tool to retrieve microbes below the skin surface. Given that MPA physical properties including size, microprojection density, length, and geometry likely influence the MPA penetration and quantity and quality of microbial extraction (25–28), we aimed to leverage on the high versatility and speed of 3D printing to fabricate transepidermal MPAs of complex, customizable designs, which are otherwise difficult to attain using conventional micromolding techniques (Fig. 1*A*). Through a systematic and iterative optimization process, we developed a standardized MPA-based sampling tool that is amenable with conventional downstream processing and analysis techniques (Fig. 1*B*) in order to reliably detect the presence of microbial colonizers in deeper layers of the skin.

Results

Optimization of 3D-Printed MPA Designs. To evaluate the impact of various physical attributes of MPAs on microbial extraction, we fabricated customized MPAs with different array sizes, densities, and geometries. Since these MPAs contained highly intricate microstructures, we chose digital light processing (DLP), a 3D printing technique that enables fast, accurate, and high-resolution printing. To comply with safety requirements necessary to perform the subsequent study on human subjects, a U.S. Food and Drug Administration (FDA) Class IIa biocompatible resin was chosen for fabrication. Cone-shaped MPAs of two different sizes (C_4 × 4, 11 × 11 mm; C_8 × 4, 22 × 11 mm) and densities (C_8 × 4, containing 32 microprojections; C_16 × 8, containing 256 microprojections) were manufactured (Fig. 2*A* and *SI Appendix*, Fig. S1), and their efficacies in capturing microbial biomass were assessed on porcine skin preloaded with *Malassezia restricta* and *Staphylococcus epidermidis ex vivo*. A 3D-printed MPA base without the microprojections was used as control. We observed that the copy numbers of both *M. restricta* and *S. epidermidis* picked up by the C_8 × 4 MPA were significantly higher than the C_4 × 4 and C_16 × 8 MPAs (Fig. 2 *B* and *C*), indicating that a larger microprojection size but lower density enhanced the extrication of both bacteria and fungi. To study the effect of microprojection geometry on the extraction efficacy, screw-shaped (S_8 × 4, 22 × 11 mm) and limpet-shaped MPAs (L_8 × 4, 22 × 11 mm) with well-defined features were printed (Fig. 2*D* and *SI Appendix*, Table S1) and applied on porcine skin as above. High-resolution scanning electron microscopy (SEM) imaging of the MPAs revealed that different microprojection geometries with high definitions were obtained (Fig. 2*E*). A generally smoother surface topography was observed in the MPA with cone geometry as compared to the screw and limpet geometries. The C_8 × 4 MPAs picked up significantly higher copy numbers of *M. restricta* compared to the L_8 × 4 counterparts. On the other hand, the *S. epidermidis* captured and identified on C_8 × 4 MPAs was superior to all other samples (Fig. 2 *F* and *G*). These results suggest that cone-shaped microprojection geometry was most effective in microbial extraction efficacy.

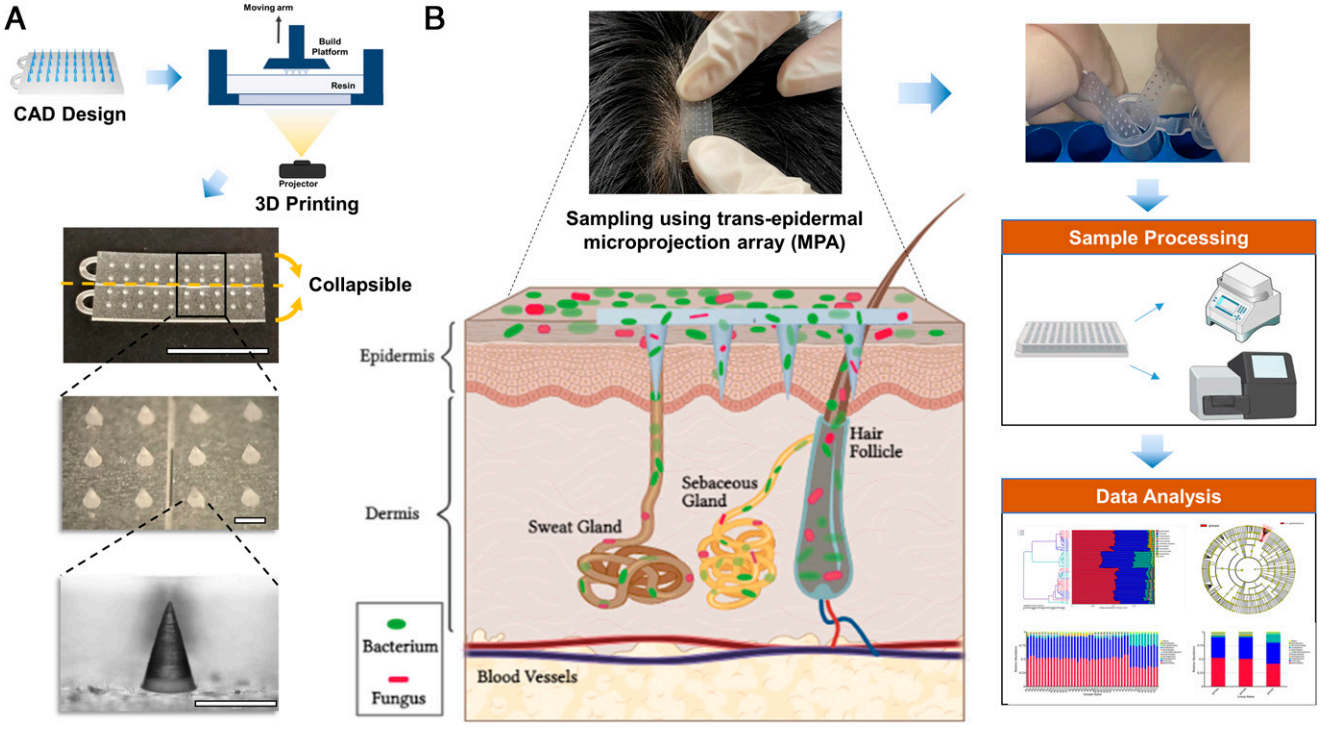

Fig. 1. Design and manufacture of the 3D-printed transepidermal MPA and the workflow for sampling of human scalp microbiome. (*A*) CAD design and 3D printing of the MPA sampling tool. Scale bar: 1 cm (*Top*), 1 mm (*Middle* and *Bottom*). (*B*) Workflow for sampling of human scalp microbiome. The MPA can be easily separated into two equal pieces and fitted into one 2-mL Eppendorf tube, which is amenable to DNA extraction using minimal buffer, thereby increasing the concentration for downstream processing by real-time PCR and amplicon sequencing.

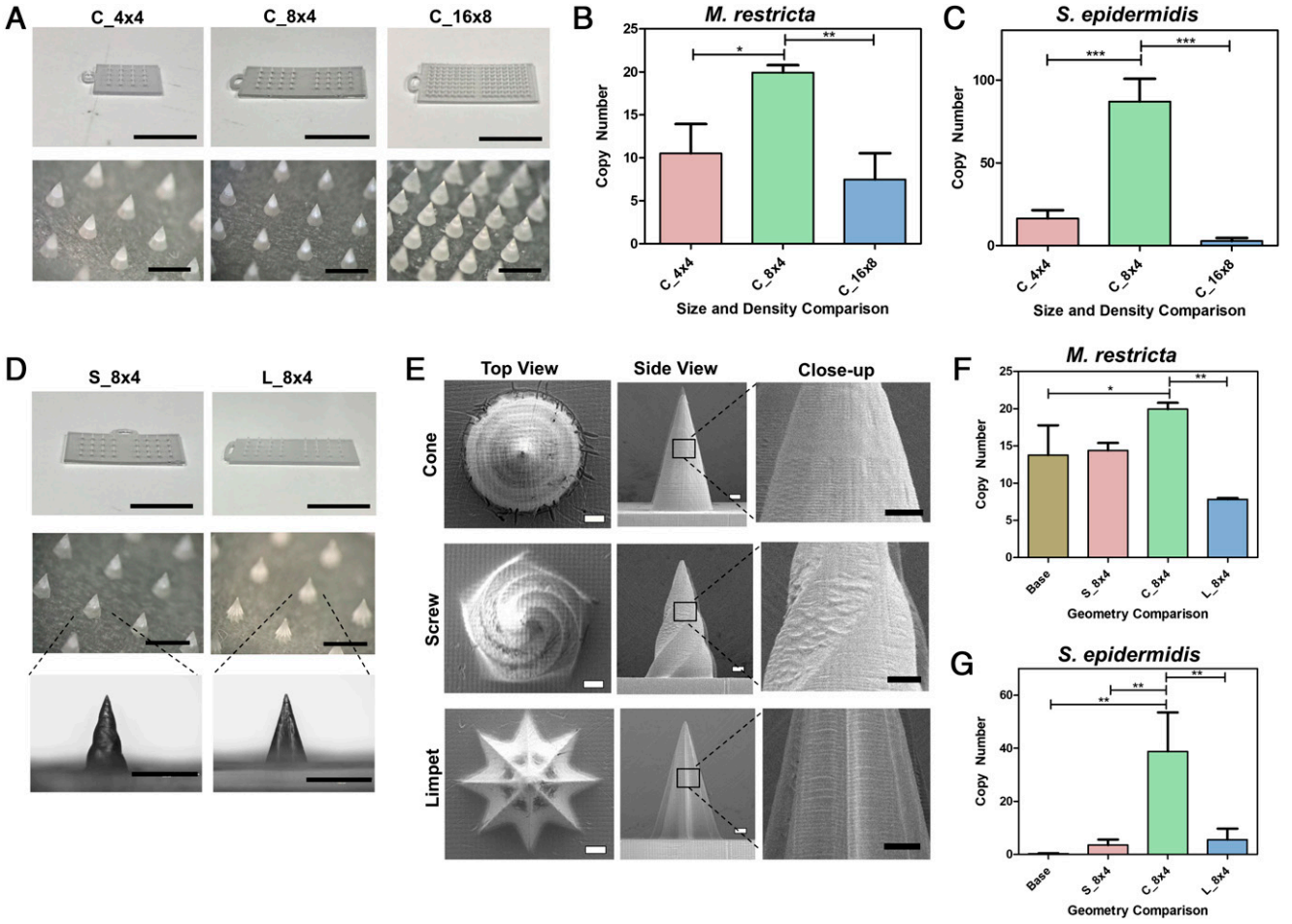

Fig. 2. Effect of MPA size, density, and geometry on microbe extraction in an *ex vivo* porcine skin model. (*A*) Microscopic images depicting the 3D-printed transepidermal MPAs of various size and density with cone-patterned microprojections. C_4 × 4: 11 × 11 mm, 4 × 4 array; C_8 × 4: 22 × 11 mm, 8 × 4 array; C_16 × 8: 22 × 11 mm, 16 × 8 array. Scale bar: 1 cm (*Top*), 1 mm (*Bottom*). Comparison of their efficacies in picking up (*B*) *M. restricta* and (*C*) *S. epidermidis* by qPCR copy number quantification. $*P < 0.05$, $**P < 0.01$, $***P < 0.001$. (*D*) Microscopic images depicting the MPAs containing microprojections of different geometries. S_8 × 4: screw-patterned, 22 mm, 8 × 4 array; L_8 × 4: limpet-patterned, 22 mm, 8 × 4 array, Scale bar: 1 cm (*Top*), 1 mm (*Middle* and *Bottom*). (*E*) High-resolution SEM images of the MPA with different microprojection geometries. Scale bar: 100 μm. Comparison of their efficacies in picking up (*F*) *M. restricta* and (*G*) *S. epidermidis* by qPCR copy number quantification. The base (22 mm) without any microprojections was used as control. $*P < 0.05$, $**P < 0.01$.

Apart from microprojection size, density, and geometry, depth of penetration is an important consideration. While longer microprojections are beneficial to extract microbial colonizers residing in the deeper layers—including SC, sebaceous glands, and hair follicles, which could extend to submillimeter depth (29)—they can lead to greater pain for subjects and higher risk of blood vessel puncture (30, 31). To strike a balance between potential discomfort and sampling of microbes in deeper skin regions, we prescreened cone-shaped MPAs comprising three different heights—1 (C_1.0), 1.2 (C_1.2), and 1.5 mm (C_1.5)—and applied them to surrogate porcine skin (*SI Appendix*, Fig. S1*A*). The histological sections depicted the cavity in the skin generated from the MPA insertion. While the highest C_1.5 MPA resulted in significantly deeper skin penetration compared to C_1.0 (244 vs. 188 μm, $P < 0.05$), there was no significant difference between C_1.2 and C_1.5 MPAs (*SI Appendix*, Fig. S1*B*). Considering that MPAs of 1.2- and 1.5-mm heights had similar microbial extraction efficacy (*SI Appendix*, Fig. S2), and given the higher risk of user discomfort and injury with the C_1.5 MPAs, C_1.2 MPAs were chosen for subsequent studies on human volunteers.

As compared to sampling on the *in vitro* porcine skin model with surface-coated microbes, detecting microbial presence in human skin requires much higher sensitivity. To reduce the extraction buffer volume required and increase sensitivity, we modified the MPA form while maintaining the optimized microprojection size (22 × 11 mm), density (8 × 4), geometry (cone), and height (1.2 mm). Instead of a solid base, we introduced perforations along the base midline to facilitate easy folding into two halves. As a result, three MPAs can be neatly fitted into one standard 2-mL Eppendorf tube (*SI Appendix*, Fig. S3). To evaluate the risks of microprojection breakage in skin, we examined MPAs post-skin application by microscopy and observed no visible fractures or structural defects (*SI Appendix*, Fig. S4*A*). The mechanical strength of the MPA was further confirmed by compression tests, which demonstrated high compressive force tolerance of >1 N/microprojection (*SI Appendix*, Fig. S4*B*) and markedly exceeded the force needed to penetrate the skin (0.15 N/microprojection) (32).

ITS and 16S Amplicon Sequencing of Scalp Microbiome from Healthy Human Subjects. Internal transcribed spacer (ITS) fungal and 16S bacterial amplicon sequencing was performed for samples collected by swabs, tape strips, and MPAs sampled from neighboring scalp regions of 29 healthy volunteers (15 males, 14 females). The swab showed a higher positive sampling rate

(i.e., extracted microbiome DNA samples that passed quality control for amplicon sequencing) for bacteria and the MPAs for fungi, respectively (Fig. 3*A*). Tape stripping yielded the lowest positive sampling rates for both bacteria and fungi.

MPA Sampling Revealed Higher Fungal Diversity and Count. Fungal species mainly from the phyla *Basidomycota* (*Malasseziomycetes*, *Agaricomycetes*) and *Ascomycota* (*Agaricomycetes*, *Saccharomycetes*, *Dothideomycetes*, *Eurotiomycetes*, *Sordariomycetes*) (Fig. 3*B* and *SI Appendix*, Fig. S6*A*) were found on scalp skin with all sampling approaches. Multiple MPA pressings (i.e., three pressings) increased the proportion of fungi detected compared to a single MPA pressing (Fig. 3*B*). Alpha and beta diversity analysis showed that MPA sampling had a higher greater species richness compared to swab (*SI Appendix*, Fig. S6 *B* and *C*), with a higher average number of observed fungal species observed with MPA than swab and tape strip (Fig. 3*C*).

The main fungal species observed remained similar across subjects, but weighted Unifrac distance analysis (which takes into account species abundance) of fungal species across different sampling methods and subjects showed that samples tended to cluster according to sampling method (Fig. 3*D*). In contrast, unweighted Unifrac distance analysis (which considers only present or absent species) was more likely to cluster samples by individual subject rather than sampling method (*SI Appendix*, Fig. S6*D*).

More species of *Basidomycota* were collected by swab as compared to MPA, whereas MPA extracted more *Ascomycota* than swab (Fig. 3*E*; *q < 0.05, **q < 0.01). To determine if MPA sampling was able to detect more clinically relevant species, we collated the average Operational Taxonomic Units (OTU) counts for reads mapping to the specific genus of interest for each respective sampling method. Significantly higher OTU counts of *Malassezia* (representative *Basidiomycota* species, $^{**}P < 0.01$) were detected in swab than MPA, whereas significantly higher OTU counts of the potentially pathogenic *Aspergillus* (representative *Ascomycota* species, $^{**}P < 0.01$) were detected in MPA as compared to swab (Fig. 3*F*). This suggests that MPA sampling may be useful for the detection of clinically relevant fungal species that cause superficial skin infection.

Swab Sampling Showed Increased Bacterial Species Number. Bacterial species mainly from the phyla *Acidobacterium*, *Actinobacterium*, *Bacteriodetes*, *Firmicutes*, and *Proteobacterium* (Fig. 4*A* and *SI Appendix*, Fig. S7*A*) were found by scalp swab sampling. Swab had a higher average number of observed bacterial species with swab than with MPA and tape strip sampling (Fig. 4*B*). No significant differences were observed in alpha and beta diversity between swab and MPA (*SI Appendix*, Fig. S7 *B* and *C*). Similar to our observations for ITS analysis, samples clustered by sampling method when measured using weighted Unifrac distance analysis and by subject when using unweighted Unifrac distance analysis (Fig. 4*C* and *SI Appendix*, Fig. S7*D*).

MPA picked up more *Firmicutes* and *Proteobacteria* than did tape stripping (Fig. 4*D*, *q < 0.05), although no significant differences were observed among all three sampling methods in terms of the OTU counts detected for representative *Firmicutes*, *Proteobacteria*, and *Mycobacterium* species (*Staphylococci*, *Pseudomonas*, and *Actinobacteria* species, respectively) (Fig. 4*E*). Overall, the most abundant five to seven fungal and bacterial species (based on OTU counts) collected from one subject were similar across all three sampling methods (*SI Appendix*, Table S2), suggesting that MPA sampling efficiency and consistency were comparable to conventional sampling tools.

Species-Specific Copy Number Enumeration by qPCR. A limitation of 16S/ITS amplicon sequencing is that it reflects only the relative abundance of the different microbial species rather than the absolute microbial load (33). Hence, for more accurate quantitation of specific microbial species, we chose to use qPCR for four representative skin commensals—*M. restricta*, *M. globosa*, *C. acnes*, and *S. epidermidis*—as these were the most frequently detected fungal and bacterial species on many healthy subjects (34, 35). Based on the availability of well-curated species-specific primers and in-house calibrated copy number vectors (36), we were able to perform species-specific qPCR quantitation for *M. restricta* ($n = 9$), *M. globosa* ($n = 8$), *P. acnes* ($n = 6$), and *S. epidermidis* ($n = 6$) on selected subject samples. Swab and tape strip samples contained more *M. restricta* compared to MPA (*SI Appendix*, Fig. S8; $^{*}P < 0.05$). No significant differences in detection were observed for *M. globosa*, *S. epidermidis*, and *C. acnes* with all three sampling approaches. In terms of fungi sampling, this result is consistent with our observations from amplicon sequencing experiments, which showed that swabbing is capturing more *Basidomycota* than MPA.

Discussion

We report a 3D-printed MPA developed to address limitations in existing skin microbiome sampling approaches and demonstrate its utility for skin microbiome sampling supplementary to swabbing and tape strip sampling approaches in healthy individuals.

3D printing for MPA fabrication was chosen as it allows rapid generation of prototypes based on computerized customizable designs. Unlike conventional micromolding and injection molding techniques used for MPA manufacture, 3D printing offers much greater versatility and complete freedom in implementing MPA design parameters by computer-aided design (CAD) software without the need of a mold template. In addition, the fabrication of complex MPA designs that would otherwise be challenging to generate by micromolding could be achieved rather easily using 3D printing (37–40). Leveraging on the speed and versatility of prototyping by 3D printing, we were able to systematically optimize the MPA design for skin microbiome sampling. First, we investigated the impact of design variables including MPA size, density, and geometries on microbe detection efficacy from skin. We noted that the extraction efficacy increased with MPA surface area (*SI Appendix*, Table S1), likely because the larger MPA provided more surface area for microbe attachment. Interestingly, increasing the transepidermal surface area did not result in higher sampling efficiency. This could be attributed to two factors. First, the extent of microprojection penetration into the skin was rather low, hence the bulk of the microprojection surface was not exposed to the microbes within the skin layers. Second, the "bed of nails" effect encountered by the MPAs with higher microprojection density (C_16 × 8) resulted in resistance to penetration due to having many microprojections located close together with little space in between (25, 41). In terms of microprojection architecture, we observed that the cone was superior to both screw and limpet geometries for microbe detection. This may be related to the surface topographies of the different geometries, as greater inhibition of bacterial adhesion had been reported on nonuniform, uneven topographies such as that of screw and limpet (Fig. 2*E*), as compared to that of the smooth cone surface (42, 43).

In the second stage, we fabricated MPA with different microprojection heights to achieve the desired skin penetration. Application on *ex vivo* porcine skin indicated that MPAs of 1.2-mm height were optimal for skin sampling, as they could reach the deeper epidermal layers and early dermal region

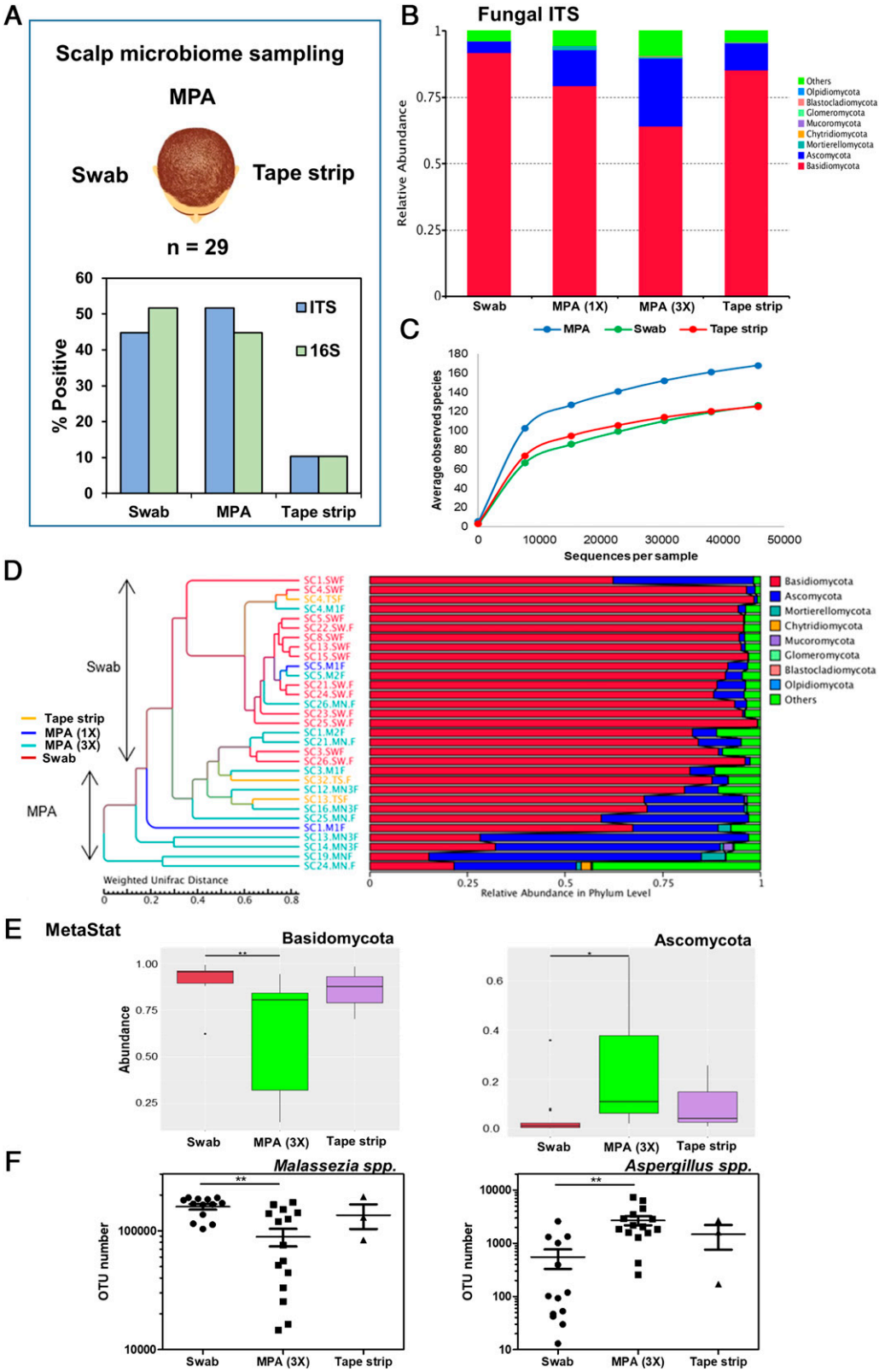

Fig. 3. Amplicon sequencing of fungal ITS regions: species comparison. (*A*) Positive sampling rate from the scalp of 29 healthy human volunteers for the detection ITS fungal and 16S bacterial amplicons, (*B*) relative abundance, and (*C*) rarefaction curves of different fungal species across different sampling approaches. (*D*) Unweighted pair group method with arithmetic mean (UPGMA) cluster tree based on weighted Unifrac distances. Clusters that segregate by sampling approach are indicated accordingly, and (*E*) Metastat analysis between groups identified *Basidomycota* and *Ascomycota* to have significant intra-group variation among the different sampling methods. *q < 0.05; **q< 0.01. (*F*) out count comparisons were performed for representative *Basidomycota* (*Malassezia*) and *Ascomycota* (*Aspergillus*) genera. A one-way ANOVA with Tukey post hoc test was used. ***P* < 0.01.

(<300 μm). Notably, the extent of needle penetration in MPA (<25%) is lower compared to other microneedles (~70%). This may be attributed to the wider base in the MPA (700-μm diameter; *SI Appendix*, Fig. S1) as compared to 300-μm conical microneedles (44). Other factors, such as thickness of skin and the application force, could also account for the differences in

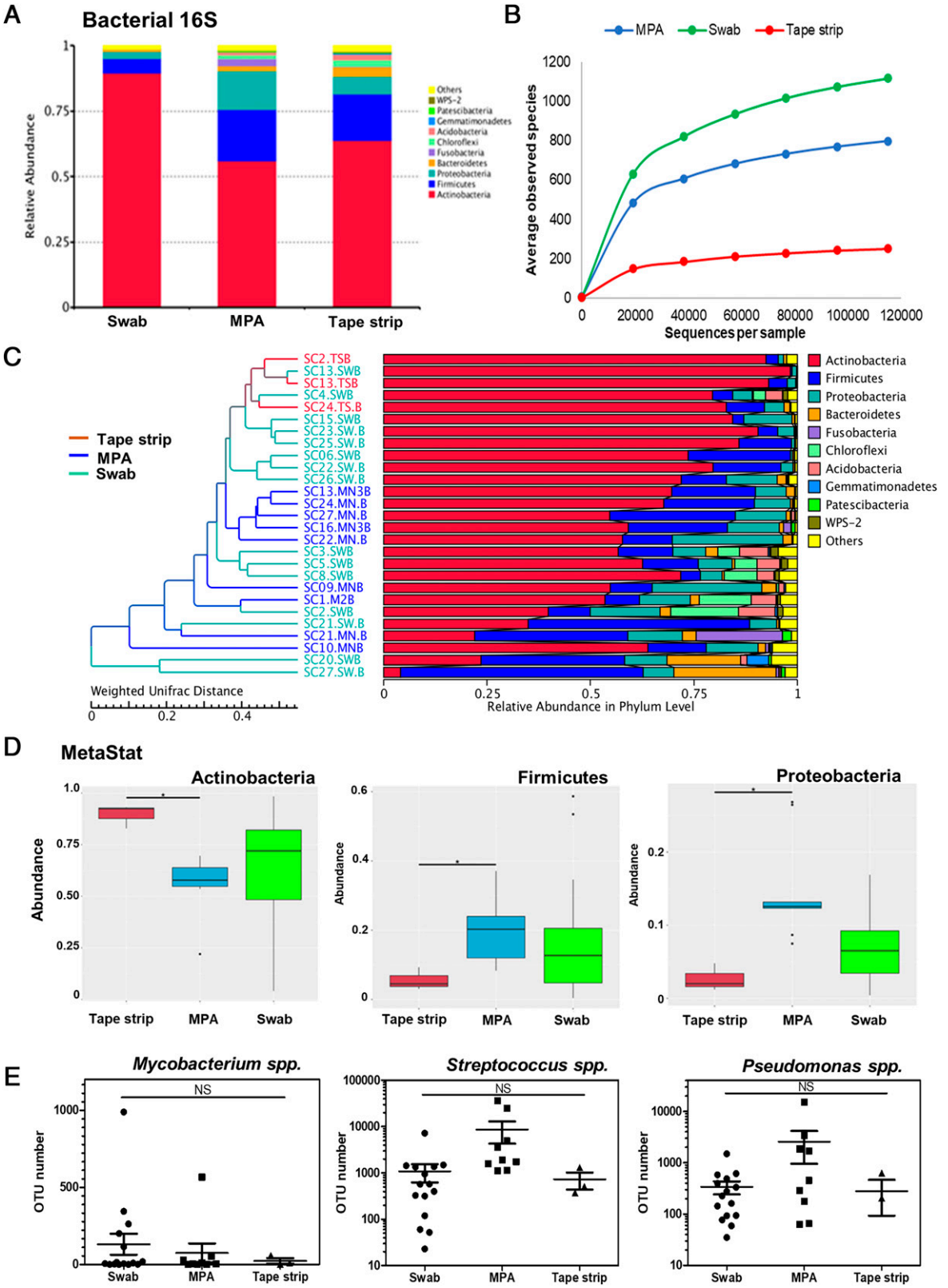

Fig. 4. Amplicon sequencing of bacterial 16S regions: species comparison. (*A*) Relative abundance and (*B*) rarefaction curves of different bacteria species across different sampling approaches. (*C*) UPGMA cluster tree based on weighted Unifrac distances. (*D*) Metastat analysis between groups identified *Actinobacteria*, *Firmicutes*, and *Proteobacteria* to have significant intragroup variation among the different sampling methods. *q < 0.05. (*E*) OTU count comparisons were performed for representative *Actinobacteria* (*Mycobacterium*), *Firmicutes* (*Streptococcus*), and *Proteobacteria* (*Psuedomonas*) genera. NS, not significant.

penetration depth (45, 46). Previous studies using microneedle-based systems have revealed that this penetration depth was associated with low or minimal pain in humans (47, 48). Nevertheless, it should be noted that the penetration study on excised skin may not truly reflect the skin condition in its native physiological environment (e.g., tensional stresses from the surrounding tissue) (31). The limited microbial biomass captured from human skin samples poses a challenge for

amplicon sequencing library construction (49, 50); therefore, in the last phase, we improved the MPA design in terms of packing efficiency to increase the detection sensitivity of downstream DNA extraction by introducing perforations on a larger MPA size to allow them to fit compactly into a 2-mL Eppendorf tube. Overall, 3D printing has enabled the rapid customization of various design parameters to facilitate the optimization of MPAs in an efficient, systematic manner.

A comparison of MPAs with conventional sampling tools on human skin revealed the optimized MPA was most effective in the detection of fungal species, while the swab was most effective for bacterial species. Both MPA and swab performed better than tape stripping, which gave the lowest positive sampling rates for bacteria and fungi. While serial tape stripping has been reported to effectively retrieve skin microbes at the buttock, back, and elbow regions (9, 51, 52), we observed limited sampling efficacy in scalp. This may be attributed to the presence of hair and high oil content on the scalp, which impeded the attachment of the tape to the scalp surface. While the superior bacterial pickup by swabbing may be attributed to the hydrophilic nature of the moistened swab, which rendered it more efficient for extraction (49, 53), it is unclear if the enhanced fungi pickup by MPA was due to better adhesion or the ability of MPAs to assess fungi-rich regions of the skin. Unlike skin surface sampling using swab or tape strip, the MPA is able to assess and extract microbes from the transepidermal (sub-200 μm) regions of the skin, as shown by the penetration studies (*SI Appendix*, Fig. S2). Since it is known that the population of microorganisms in skin changes with skin depth (7, 12), we believe that the differences in microbes collected between MPA and swab or tape strip are most likely due to the inherent species differences across skin depth. Further studies using deep skin harvesting techniques, such as skin biopsies, would be required to validate the relative abundance of fungi in the deeper epidermal layers, taking into account various factors including study design (e.g., cohort size, disease/healthy subjects, geographical region), the sampling region, sample processing techniques, and data analysis methods (15).

The effective fungi detection by MPA could aid the diagnosis of diseases caused by pathogenic microbes. Clinically, MPA microbiome sampling may be especially useful in supporting the diagnosis of invasive superficial mycoses or cellulitis, as the pathogenesis of many of these skin conditions involves microbe colonization beyond the skin surface and, hence, would require depth sampling for accurate detection. In our study, we observed that MPA sampling was significantly better at picking up *Ascomycota*, which is a phylum comprising many opportunistic pathogens including *Candida spp*, *Aspergillus spp*, *Acremonium spp*, *Microascus brevicaulis*, and *Scytalidinum dimidiatum* (54, 55). If these fungi were preferentially colonizing the deeper skin layers, it would pave the way for future therapeutic strategies such as the incorporation of antifungal agents in the MPAs for targeted localized delivery (56).

Apart from improved detection of fungal abundance and clinical relevance, our MPA sampling approach offered several advantages over swab and tape strip. MPA is applicable across nonstandard skin surfaces and can be tailored to accommodate larger skin surfaces that may be curved/contoured (57, 58). In addition, the easy customizability of microprojection height enables sampling of skin from body sites of varying epidermal thickness (59). The MPA may not replace existing sampling methods, but it serves as an additional tool in our arsenal of sampling methods to be used as deemed relevant by the investigator (e.g., if an invasive skin infection is suspected to be caused by an *Ascomycota* species).

In conclusion, we have developed a human skin microbiome sampling tool based on a unique, optimized MPA design enabled by 3D printing. In terms of sensitivity of human scalp sampling, MPA was superior to tape strip and comparable to swab. Among all the approaches, MPA yielded samples with greater fungal diversity and had a higher sensitivity for members of the *Ascomycota* phylum, probably due to its ability to assess deeper layers of the skin. Our findings demonstrated the efficacy of MPA as a human microbiome sampling tool, which will be complementary to existing sampling methods and will aid in our understanding of the human skin microbiome in health and disease.

Materials and Methods

Reagents. The DLP printing resin (freeprint ortho, DETAX) and isopropyl alcohol (IPA) (99.9% vol/vol) were purchased from Eye-2-Eye Communications Pte Ltd, Singapore. The resin composition is (% wt/wt) 20 to 50% isopropylidenediphenol PEG-2 dimethacrylate, 10 to 25% urethane dimethacrylate, 5 to 25% 1,12-dodecanediol dimethacrylate, <5% hydroxypropyl methacrylate, 1 to 10% tetrahydrofurfuryl methacrylate, 0.1 to 5% diphenyl (2,4,6-trimethylbenzoyl) phosphine oxide, and <1% 2-hydroxyethyl methacrylate. The optimal cutting temperature (OCT) compound was acquired from Tissue-tek (Sakura Finetek, Torrance, CA). PCR reagents and proteinase K were purchased from Sigma-Aldrich, Singapore.

Design and Manufacture of MPAs. The MPAs were fabricated using a DLP printer (Max × 27 ultraviolet [UV], Asiga) and a commercial FDA Class IIa biocompatible resin: FREEPRINT Ortho, which has high optical transparency for visualization and allows for high-resolution printing. The MPAs were designed using CAD software TinkerCAD and Blender. Surface area calculations of the MPAs were performed using the Blender software. Subsequently, Asiga Composer software was used to process the .stl files and adjust the printing parameters to achieve the desired printing resolution. Following DLP printing, the MPAs were washed in IPA for 5 min in a sonicator bath to remove any uncured resin and cured in a UV chamber for 20 min to ensure complete photopolymerization. The close-up microprojection features of MPAs were imaged using a light microscope (EVOS 5000M, Thermofisher Scientific).

Name	Length (cm)	Width (cm)	No. microprojections	MPA height (mm)	MPA spacing (mm)	MPA geometry
C_11_4x4	11	11	16	1.5	2	cone
C_22_8x4	22	11	32	1.5	2	cone
C_22_16x8	22	11	128	1.5	1.2	cone
S_22_8x4	22	11	32	1.5	2	screw
L_22_8x4	22	11	32	1.5	2	limpet
C_1.0	22	11	32	1.0	2	cone
C_1.2	22	11	32	1.2	2	cone
C_1.5	22	11	32	1.5	2	cone
Final MPA	22	10	40	1.2	2	cone

The dimensions of the printed MPA prototypes are listed in the table below:

SEM Imaging. MPAs of various geometries were affixed onto a sticky tape, sputter-coated with 4-nm-thickness platinum (Leica EM SCD500), and examined by SEM (JSM-6701F, JEOL, Japan).

Fracture Test. MPA fracture tests were conducted using an Instron 6800. Samples were placed pointed-side up on the stage and compressed with a 10-kN load cell at 1 mm/min up to 50 N applied force.

Histology Analyses. Skin penetration by MPAs was evaluated by analyzing the histological sections of porcine skin *ex vivo* after application with MPAs (pressed by hand ~5 s). The insertion site on the skin surface was exposed to Tryphan Blue (0.4 wt%) dye for 1 min before embedding in an OCT compound for cryosection. The frozen OCT skin samples were then sliced into 5-μm-thick sections using a cryotome (Leica CM3050 S) and analyzed using an inverted fluorescence microscope (Olympus CX41). The depth of MPA penetration, defined as the distance from lowest point in the cavity to the skin surface, was quantitatively measured using the image analysis software Fiji.

Culture of Bacteria and Fungi for Mock Community Testing. Bacteria reference strains (*S. epidermidis* ATCC 12228, *S. aureus* ATCC 29213) were cultured in Luria broth with overnight shaking at 37 °C. *Malassezia* reference strains (*M. restricta* CBS 7877, *M. globosa* CBS 7966, *M. sympodialis* CBS 7222) were cultured in mDixon broth at 32 °C to confluence. For the reconstitution of a mock community, 5 mL microbial suspension was prepared with a final OD_{600} of 0.1 for bacterial species and 0.05 for *Malassezia* species, spread evenly on the surface of a 6 cm × 6 cm piece of porcine skin, and incubated for 15 min. The excess suspension solution was then decanted, and the skin was left to air dry for an additional 15 min.

Skin Sampling and DNA Extraction. The study design and full protocol involving human scalp sampling was reviewed and approved by the Agency for Science, Technology and Research (A*STAR) Human Biomedical Research office under the approval code #2019–003, with written informed consent from all subjects. All subjects provided written informed consent prior to commencement of the study. Participants were between 22 and 65 y of age and judged to be healthy based on the absence of overt skin diseases. A total of 29 (14 female, 15 male) healthy subjects were recruited for this study. Human and porcine skin microbiome sampling was performed using the COPAN FLOQswab (COPAN Italia, Brescia, Italy), D-Squame standard sampling discs (Cuderm Cooporation, Dallas, TX)/tape strip, or the abovementioned MPAs. Briefly, swabbing was performed by wetting the swab with sterile saline and swabbing an area of the skin ~4.0 cm^2 back and forth thrice. In total, 25 single spot pressings of one tape strip were used for each sampling. MPAs were applied in one or three pressings (MPA 1× or 3×) per sampling at different sampling regions, and the data shown are all 3× by default unless specified otherwise. Immediately after sampling, each swab/tape strip/MPA was placed in an Eppendorf tube containing universal DNA extraction buffer containing 20 μg/mL proteinase K (Sigma-Aldrich, Singapore) and incubated at 56 °C for 12 to 18 h. Following proteinase K inactivation (94 °C, 5 min) and high-speed centrifugation, the supernatant was collected and processed for downstream analysis.

qPCR Detection and Quantification. Real-time qPCR was performed with species-specific primers for bacterial and fungi (*SI Appendix*, Table S3) using the Luna universal qPCR master mix (NEB, Singapore) alongside species-specific pCR4 plasmid template standard curves (3 to 3,000,000 copies) constructed for the respective species amplicons. Statistical analyses were performed using one-way ANOVA followed by Tukey's post hoc test (*$P < 0.05$, **$P < 0.01$, ***$P < 0.001$).

18S and 16S Amplicon Sequencing. gDNA extraction from swabs, MPAs, and tape strips was performed as described above. DNA concentration and quality were assessed photometrically using a NanoDrop ND-2000c UV–vis spectrophotometer (NanoDrop Technologies, Wilmington, DE). The primer set 341F (5′-CCT AYG GGR BGC ASC AG-3′) and 806R (5′-GGA CTA CNN GGG TAT CTA A -3′) was used for the amplification of the V3-V4 region of bacterial 16S ribosomal ribonucleic acid (rRNA) gene. The primer set ITS5 (5′- GGA AGT AAA AGT CGT AAC AAG G-3′) and ITS2 (5′- GCT GCG TTC TTC ATC GAT GC -3′) was used for the amplification of the ITS region of fungal 18S rRNA gene. The libraries were sequenced on IlluminaHiSeq platform 2500, and 250-bp paired-end reads were generated at Novogene AIT (Singapore). Assigned paired-end reads of each sample were merged to raw tags by using Fast Length Adjustment of SHort reads (FLASH) (version 1.2.7), and the merged raw tags were filtered and developed into clean tags according to Quantitative Insights Into Microbial Ecology (QIIME) (version 1.7.0). MUltiple Sequence Comparison by Log-Expectation (MUSCLE) (version 3.8.31) was used to obtain the phylogenetic relationship of all OTU representative sequences. Alpha and beta diversity indices were calculated with QIIME (version 1.7.0).

Statistical Analysis. All the data reported in this study were the means ± SD. Statistical analysis was performed using one-way ANOVA with Tukey's multiple comparisons test, unpaired *t* test, and Wilcoxon signed-rank test with Prism 5 software (GraphPad). A *P* value and q value of < 0.05 was considered to be statistically significant.

Data Availability. All study data are included in the article and/or *SI Appendix*.

16S and ITS amplicon sequencing data are available in the National Center for Biotechnology Information (NCBI) database under the Sequence Read Archive BioProject ID PRJNA856066 (60).

ACKNOWLEDGMENTS. This work was supported by the National Additive Manufacturing Innovation Cluster@NTUitive (NAMIC@NTUitive), Singapore, grants 2018255 and 2019060. Authors were supported by funding from A*STAR and A*STAR BMRC EDB IAF-PP grants H17/01/a0/004 "Skin Research Institute of Singapore" (K.L. and T.L.D.J.) and H18/01a0/016 "Asian Skin Microbiome Program" (C.L., N.C., Y.I.L., and T.L.D.J.). H.L.T. was supported by Singapore Ministry of Health's National Medical Research Council under its Clinician Scientist Award (CSAINV20nov-0003).

1. Y. E. Chen, M. A. Fischbach, Y. Belkaid, Skin microbiota-host interactions. *Nature* **553**, 427–436 (2018).
2. S. Ryu, P. I. Song, C. H. Seo, H. Cheong, Y. Park, Colonization and infection of the skin by *S. aureus*: Immune system evasion and the response to cationic antimicrobial peptides. *Int. J. Mol. Sci.* **15**, 8753–8772 (2014).
3. M. M. Pettigrew, J. K. Johnson, A. D. Harris, The human microbiota: Novel targets for hospital-acquired infections and antibiotic resistance. *Ann. Epidemiol.* **26**, 342–347 (2016).
4. J. R. Köhler, B. Hube, R. Puccia, A. Casadevall, J. R. Perfect, "Fungi that infect humans" in *The Fungal Kingdom*, J. Heitman et al., Eds. (Wiley, 2017).
5. M. R. Williams, R. L. Gallo, Evidence that human skin microbiome dysbiosis promotes atopic dermatitis. *J. Invest. Dermatol.* **137**, 2460–2461 (2017).
6. E. A. Grice, J. A. Segre, The skin microbiome. *Nat. Rev. Microbiol.* **9**, 244–253 (2011).
7. A. L. Byrd, Y. Belkaid, J. A. Segre, The human skin microbiome. *Nat. Rev. Microbiol.* **16**, 143–155 (2018).
8. L. Bay *et al.*, Universal Dermal Microbiome in Human Skin. *mBio* **11**, e02945-19 (2020).
9. P. L. Zeeuwen *et al.*, Microbiome dynamics of human epidermis following skin barrier disruption. *Genome Biol.* **13**, R101 (2012).
10. B. Lange-Asschenfeldt *et al.*, Distribution of bacteria in the epidermal layers and hair follicles of the human skin. *Skin Pharmacol. Physiol.* **24**, 305–311 (2011).
11. T. Nakatsuji *et al.*, *Staphylococcus aureus* exploits epidermal barrier defects in atopic dermatitis to trigger cytokine expression. *J. Invest. Dermatol.* **136**, 2192–2200 (2016).
12. T. Nakatsuji *et al.*, The microbiome extends to subepidermal compartments of normal skin. *Nat. Commun.* **4**, 1431 (2013).
13. X. Huang *et al.*, Murine model of colonization with fungal pathogen *Candida auris* to explore skin tropism, host risk factors and therapeutic strategies. *Cell Host Microbe* **29**, 210–221.e6 (2021).
14. S. Prast-Nielsen *et al.*, Investigation of the skin microbiome: Swabs vs. biopsies. *Br. J. Dermatol.* **181**, 572–579 (2019).
15. H. H. Kong *et al.*, Performing skin microbiome research: A method to the madness. *J. Invest. Dermatol.* **137**, 561–568 (2017).
16. O. A. Alexeyev, Bacterial landscape of human skin: Seeing the forest for the trees. *Exp. Dermatol.* **22**, 443–446 (2013).
17. B. Dréno *et al.*, Microbiome in healthy skin, update for dermatologists. *J. Eur. Acad. Dermatol. Venereol.* **30**, 2038–2047 (2016).
18. E. A. Grice *et al.*; NISC Comparative Sequencing Program, A diversity profile of the human skin microbiota. *Genome Res.* **18**, 1043–1050 (2008).
19. A. S. Rzhevskiy, T. R. R. Singh, R. F. Donnelly, Y. G. Anissimov, Microneedles as the technique of drug delivery enhancement in diverse organs and tissues. *J. Control. Release* **270**, 184–202 (2018).
20. L. Zhao *et al.*, Smart responsive microarray patches for transdermal drug delivery and biological monitoring. *Adv. Healthc. Mater.* **10**, e2100996 (2021).
21. R. S. J. Ingrole *et al.*, Trends of microneedle technology in the scientific literature, patents, clinical trials and internet activity. *Biomaterials* **267**, 120491 (2021).
22. H. Chang *et al.*, A swellable microneedle patch to rapidly extract skin interstitial fluid for timely metabolic analysis. *Adv. Mater.* **29**, 1702243 (2017).
23. P. P. Samant, M. R. Prausnitz, Mechanisms of sampling interstitial fluid from skin using a microneedle patch. *Proc. Natl. Acad. Sci. U.S.A.* **115**, 4583–4588 (2018).

24. J. Zhu *et al.*, Gelatin methacryloyl microneedle patches for minimally invasive extraction of skin interstitial fluid. *Small* **16**, e1905910 (2020).
25. P. Makvandi *et al.*, Engineering microneedle patches for improved penetration: Analysis, skin models and factors affecting needle insertion. *Nano-Micro Lett.* **13**, 93 (2021).
26. C. Yeung *et al.*, A 3D-printed microfluidic-enabled hollow microneedle architecture for transdermal drug delivery. *Biomicrofluidics* **13**, 064125 (2019).
27. W.-G. Bae *et al.*, Snake fang-inspired stamping patch for transdermal delivery of liquid formulations. *Sci. Transl. Med.* **11**, eaaw3329 (2019).
28. A. P. Raphael *et al.*, Formulations for microprojection/microneedle vaccine delivery: Structure, strength and release profiles. *J. Control. Release* **225**, 40–52 (2016).
29. K. Polak-Witka, L. Rudnicka, U. Blume-Peytavi, A. Vogt, The role of the microbiome in scalp hair follicle biology and disease. *Exp. Dermatol.* **29**, 286–294 (2020).
30. H. S. Gill, D. D. Denson, B. A. Burris, M. R. Prausnitz, Effect of microneedle design on pain in human volunteers. *Clin. J. Pain* **24**, 585–594 (2008).
31. S. A. Coulman *et al.*, In vivo, in situ imaging of microneedle insertion into the skin of human volunteers using optical coherence tomography. *Pharm. Res.* **28**, 66–81 (2011).
32. W. Li *et al.*, Rapidly separable microneedle patch for the sustained release of a contraceptive. *Nat. Biomed. Eng.* **3**, 220–229 (2019).
33. F. A. Tettamanti Boshier *et al.*, Complementing 16S rRNA gene amplicon sequencing with total bacterial load to infer absolute species concentrations in the vaginal microbiome. *mSystems* **5**, e00777-19 (2020).
34. T. L. Dawson Jr., *Malassezia globosa* and *restricta*: Breakthrough understanding of the etiology and treatment of dandruff and seborrheic dermatitis through whole-genome analysis. *J. Investig. Dermatol. Symp. Proc.* **12**, 15–19 (2007).
35. J.-P. Claudel *et al.*, *Staphylococcus epidermidis*: A potential new player in the physiopathology of acne? *Dermatology* **235**, 287–294 (2019).
36. C. Leong *et al.*, Effect of zinc pyrithione shampoo treatment on skin commensal *Malassezia*. *Med. Mycol.* **59**, 210–213 (2021).
37. D. Han *et al.*, 4D printing of a bioinspired microneedle array with backward-facing barbs for enhanced tissue adhesion. *Adv. Funct. Mater.* **30**, 1909197 (2020).
38. S. N. Economidou *et al.*, 3D printed microneedle patches using stereolithography (SLA) for intradermal insulin delivery. *Mater. Sci. Eng. C* **102**, 743–755 (2019).
39. C. Caudill *et al.*, Transdermal vaccination via 3D-printed microneedles induces potent humoral and cellular immunity. *Proc. Natl. Acad. Sci. U.S.A.* **118**, 1–8 (2021).
40. H. Derakhshandeh *et al.*, A wirelessly controlled smart bandage with 3D-printed miniaturized needle arrays. *Adv. Funct. Mater.* **30**, 1–11 (2020).
41. S. H. Lim *et al.*, Geometrical optimisation of a personalised microneedle eye patch for transdermal delivery of anti-wrinkle small peptide. *Biofabrication* **12**, 035003 (2020).
42. N. Lu *et al.*, Fabrication of PDMS surfaces with micro patterns and the effect of pattern sizes on bacteria adhesion. *Food Control* **68**, 344–351 (2016).
43. S. Perni, P. Prokopovich, Micropatterning with conical features can control bacterial adhesion on silicone. *Soft Matter* **9**, 1844–1851 (2013).
44. Y. Li *et al.*, Dissolving microneedle arrays with optimized needle geometry for transcutaneous immunization. *Eur. J. Pharm. Sci.* **151**, 105361 (2020).
45. S. A. Ranamukhaarachchi *et al.*, A micromechanical comparison of human and porcine skin before and after preservation by freezing for medical device development. *Sci. Rep.* **6**, 32074 (2016).
46. R. F. Donnelly *et al.*, Optical coherence tomography is a valuable tool in the study of the effects of microneedle geometry on skin penetration characteristics and in-skin dissolution. *J. Control. Release* **147**, 333–341 (2010).
47. S. Sharma *et al.*, A pilot study in humans of microneedle sensor arrays for continuous glucose monitoring. *Anal. Methods* **10**, 2088–2095 (2018).
48. A. Ripolin *et al.*, Successful application of large microneedle patches by human volunteers. *Int. J. Pharm.* **521**, 92–101 (2017).
49. G. Finazzi, M. N. Losio, G. Varisco, FLOQSwab™: Optimisation of procedures for the recovery of microbiological samples from surfaces. *Ital. J. Food Saf.* **5**, 5756 (2016).
50. R. D. Bjerre *et al.*, Effects of sampling strategy and DNA extraction on human skin microbiome investigations. *Sci. Rep.* **9**, 17287 (2019).
51. K. Ogai *et al.*, A comparison of techniques for collecting skin microbiome samples: Swabbing versus tape-stripping. *Front. Microbiol.* **9**, 2362 (2018).
52. K. R. Chng *et al.*, Whole metagenome profiling reveals skin microbiome-dependent susceptibility to atopic dermatitis flare. *Nat. Microbiol.* **1**, 16106 (2016).
53. L. Jansson, Y. Akel, R. Eriksson, M. Lavander, J. Hedman, Impact of swab material on microbial surface sampling. *J. Microbiol. Methods* **176**, 106006 (2020).
54. J. J. Limon, J. H. Skalski, D. M. Underhill, Commensal fungi in health and disease. *Cell Host Microbe* **22**, 156–165 (2017).
55. M. Sandoval-Denis *et al.*, *Scopulariopsis*, a poorly known opportunistic fungus: Spectrum of species in clinical samples and in vitro responses to antifungal drugs. *J. Clin. Microbiol.* **51**, 3937–3943 (2013).
56. P. Zan *et al.*, Antimicrobial microneedle patch for treating deep cutaneous fungal infection. *Adv. Ther.* **2**, 1–7 (2019).
57. H. Wang, G. Pastorin, C. Lee, Toward self-powered wearable adhesive skin patch with bendable microneedle array for transdermal drug delivery. *Adv. Sci. (Weinh.)* **3**, 1500441 (2016).
58. S. H. Lim, J. Y. Ng, L. Kang, Three-dimensional printing of a microneedle array on personalized curved surfaces for dual-pronged treatment of trigger finger. *Biofabrication* **9**, 015010 (2017).
59. J. Sandby-Møller, T. Poulsen, H. C. Wulf, Epidermal thickness at different body sites: Relationship to age, gender, pigmentation, blood content, skin type and smoking habits. *Acta Derm. Venereol.* **83**, 410–413 (2003).
60. K. Liang *et al.*, Human scalp microbiome sampling. NCBI-SRA. https://www.ncbi.nlm.nih.gov/sra/?term=856066. Deposited 6 July 2022.